Available online at www.sciencedirect.com

ScienceDirect

Physics Procedia 56 (2014) 29 – 39

Physics Procedia

8th International Conference on Photonic Technologies LANE 2014

Electro-optic and acousto-optic laser beam scanners - Invited Paper -

G.R.B.E. Römer[a,*], P. Bechtold[b,c]

[a] University of Twente, Chair of Applied Laser Technology, Drienerlolaan 5, Enschede, 7522NB, The Netherlands
[b] Institute of Photonic Technologies, Friedrich-Alexander-Universität Erlangen-Nürnberg, Paul-Gordan-Str. 3, 91052 Erlangen, Germany
[c] Erlangen Graduate School in Advanced Optical Technologies (SAOT), Friedrich-Alexander-Universität Erlangen-Nürnberg, Paul-Gordan-Str. 6, 91052 Erlangen, Germany

Abstract

Optical solid state deflectors rely on the electro-optical or acousto-optic effect. These Electro-Optical Deflectors (EODs) and Acousto-Optical Deflectors (AODs) do not contain moving parts and therefore exhibit high deflection velocities and are free of drawbacks associated with mechanical scanners. A description of the principles of operation of EODs and AODs is presented. In addition, characteristics, properties and the (dis)advantages of EODs and AODs, when compared to mirror based mechanical deflectors, is discussed. Deflection angles, speed and accuracy are discussed in terms of resolvable spots and related quantities. Also, response time, damage threshold, efficiency and the type and magnitude of beam distortions is addressed. Optical deflectors are characterized by high angular deflection velocities, but small deflection angles. Whereas mechanical mechanical scanners are characterized by relatively small deflection velocities, but large deflection angles. Arranging an optical deflector and a mechanical scanner in series allows to take advantage of the best of both worlds.

Peer-review under responsibility of the Bayerisches Laserzentrum GmbH
Keywords: laser beam scanner ; mirror-based deflection; optical solid state deflectors; electro-optical deflector; acousto-optical deflector; large stroke small stroke

1. Introduction

Laser beam scanners, or laser beam deflectors, have a wide range of scientific and industrial applications, such as fluorescence microscopy, optical storage, laser printers, display, sensing and laser material processing. These laser scanners are used to deflect the laser beam, in order to position the laser spot, in one, two, or even three dimensions, on (or below) the surface of the substrate under consideration. To reduce processing time, high speed beam deflection is of interest for microscopy applications, such as random-access fluorescence microscopy (Bullen et al., 1997) and swept-source optical coherence tomography (Okabe et al., 2013), but also for high-power, high-repetition-rate laser-material processing using ultra short laser pulses (Bruening et al., 2011; Schille et al., 2008). Regarding the latter application, the pulse frequencies of ultra short pulsed laser sources has been significantly increasing over the years to

* Corresponding author. Tel.: +31-53-489-2519 ; fax: +31-53-489-3631.
E-mail address: g.r.b.e.romer@utwente.nl

Peer-review under responsibility of the Bayerisches Laserzentrum GmbH
doi:10.1016/j.phpro.2014.08.092

values over 10 MHz . To fully exploit the capabilities of these laser sources in these applications, the beam deflection velocity is to be in the order of focal spot diameter (typically 100 μm or less) multiplied by the laser pulse frequency, resulting in beam defection angle velocities in the order of 1000 rad/s. Unfortunately, the deflection angle velocities of frequently used servo-controlled Galvanometer-based scanners are typically 100 rad/s or less (Bechtold et al., 2013b).

The deflection angle velocities of these Galvo-scanners, and other mirror based scanners, such as piezo scanners (PI, 2014), and Micro-Electro-Mechanical Systems (MEMS) scanners (Piyawattanametha et al., 2005; Yalcinkaya et al., 2006; Ferreira and Moehlecke, 1999) are fundamentally limited by the inertia associated with the mass of the rotating mirror and other moving parts. Hence, to exploit the capabilities of high-pulse frequency laser sources, other *high-speed* beam deflection technologies have to be considered, which may be loosely grouped into two categories: *mirror based mechanical deflectors* and *optical solid state deflectors*, see Fig. 1. High-speed mirror based deflection technologies include rotating polygon wheel scanners (De Loor, 2013), and resonant scanners, such as resonant piezo scanners (PI, 2014), and resonant MEMS scanners (Piyawattanametha et al., 2005; Yalcinkaya et al., 2006; Ferreira and Moehlecke, 1999). The latter type of scanners achieve high beam deflection velocities and large deflection angles, by operating the mechanism, including the mirror, in its Eigenfrequency. In essence, polygon and resonant scanners are *raster scanning* technologies, in which the laser beam is scanned over the substrate line by line in a raster pattern, causing pixelation. In this approach, the laser power is to be modulated and synchronized to the laser pulse frequency, in order to deliver the desired energy dose at the desired location on the substrate. In most cases, the entire scan area needs to be scanned. In contrast to raster scanning, *vector scanning*, or *random-access scanning*, allows to scan the laser beam along a trajectory where the laser energy actually needs to be delivered to the substrate, rather than scanning the entire area. Vector scanning can provide a higher spatial resolution, as well as a reduction in the total processing time, when compared to raster scanning.

	Deflection speed	
Scan type	*Low*	*High*
Raster scanning		Polygon wheel & resonant scanners
Random-access scanning	Galvano-, piezo- & MEMS scanners	Optical deflectors (EODs & OADs)

Fig. 1. Categories of laser beam scanner technologies.

As photons are massless, deflection by “mass free” technologies – i.e. technologies without moving parts – are preferred over rotating-mirror based mechanical deflectors. Optical solid state deflectors, which rely on the *electro-optical* or *acousto-optic effect*, are deflectors, which do not contain moving parts and therefore can exhibit high deflection angle velocities. Moreover, these *Electro-Optical Deflectors* (EODs) and *Acousto-Optical Deflectors* (AODs) are free of drawbacks associated with mechanical scanners, such as wear and tear, mechanical noise and drift. Moreover, EODs and AODs allow random-access scanning.

This paper provides a basic description of the principle of operation of EODs and AODs, as well as an overview of their characteristics, properties and the (dis)advantages as a laser beam deflector, when compared to mirror based mechanical deflectors, see Table 1. Although EODs and AODs can and are employed in various scanner applications, the main focus in this paper is on the use of EODs and AODs for laser materials processing. To that end, first scanner performance criteria, in terms of *resolvable spots*, and related quantities, are defined in section 2. Next, in section 3, EODs are discussed. AODs are discussed in section 4. Section 5, discusses a combination of an optical solid state deflector and a random-access Galvo-scanner, exploiting the merits of both deflection technologies. Finally, section 6 concludes with a summary.

2. Performance criteria

The main quantities defining the performance of a laser beam deflector are the *maximum deflection angle* θ [rad], the *maximum deflection angle velocity* $\dot{\theta}$ [rad/s] and the *angular accuracy of deflection* $\Delta\theta$ [rad]. Unfortunately, the different deflection technologies are usually specified by disparate parameters. Translating these parameters into maximum deflection angle, angle velocity and angular accuracy is possible, but not sufficient for an objective evaluation

Table 1. Properties* (typical values) and comparison of laser beam scanners for a near-infrared wavelength.

Scanning technology	Aperture [mm]	Max. deflection angle θ [rad] (Number of resolvable spots N)	Max. velocity $\dot{\theta}$ [10^3 rad/s] (Rate of resolvable spots $\dot{N}$ [10^6])	Accuracy $\Delta\theta$ [μrad] (Accuracy per resolvable spot [%])	Response time τ [μs]	Efficiency or Transparency
Galvo scanner	7 . . . 30	0.5 . . . 1 (3000 . . . 18000)	~ 0.1 (0.5 . . . 1)	< 2 (< 5)	~ 10^3	> 95%
Polygon scanner	2 . . . 12	0.6 . . . 1 (2000 . . . 7000)	1 . . . 10 (5 . . . 40)	~ 200 (~ 120)	$\gg 10^3$	> 90%
Piezo scanner	10 . . . 25	0.01 . . . 0.1 (100 . . . 1000)	0.01 . . . 0.1 (0.1 . . . 1)	~ 1 (~ 1)	~ 10^3	> 95%
MEMS scanner – static	1 . . . 2.5	~ 0.5 (200 . . . 1000)	0.1 . . . 1 (0.1 . . . 1)	n.a.	~ 10^3	> 90%
MEMS scanner – resonant	~ 1	0.5 . . . 1 (500 . . . 1000)	10 . . . 30 (5 . . . 20)	n.a.	$\gg 10^3$	> 90%
EOD (Pockels effect)	2	~ 0.001 (2)	2 . . . 20 (3 . . . 30)	~ 1 (~ 0.2)	0.04 . . . 1	> 85%
EOD (Kerr effect, KTN)	0.5	~ 0.2 (50)	~ 40 (15)	n.a.	~ 10	> 90%
AOD	1 . . . 10	0.01 . . . 0.05 (10 . . . 500)	5 . . . 250 (20 . . . 80)	$\ll 0.1$ ($\ll$0.1)	0.5 . . . 15	60% . . . 80%

*Data according to official information by Cambridge Technology Inc., Scanlab AG, Raylase AG, Piezosystem Jena GmbH, Physik Instrumente (PI) GmbH & Co. KG, Fraunhofer-Institut IPMS, Lemoptix SA, Adriatic Research Institute, Hamamatsu Photonics K.K., AA Opto-Electronic Company, Gooch & Housego, Brimrose Corp., Isomet Corp., IntraAction Corp., NTT Advanced Technology Corp. and Conoptics Inc.

and comparison of the different technologies (Bechtold et al., 2013b). Moreover, because the typical aperture (size), as well as the maximum deflection angle of optical deflectors is small, the diameter and far-field full divergence angle θ_{div} of the laser beam being deflected, limit the resolution of the deflector. That is, the beam diameter (waist) is to be reduced to match the aperture size of the optical deflector, implying an increase of the beam divergence. The latter is dictated by the invariance of the *waist-divergence product*, which is characteristic for a laser beam (Bass, 2010). That is, especially in the case of small apertures and small deflection angles, the maximum deflection angle may be in the same order of magnitude of the divergence angle of the laser beam. Therefore, *the number of resolvable spots N*, defined as

$$N = \frac{\theta}{\theta_{\mathrm{div}}} \tag{1}$$

i.e. the factor by which the maximum deflection angle θ exceeds the beam divergence angle θ_{div}, is an objective parameter to allow comparison of the maximum deflection angles of different technologies. This quantity can also be understood as the *resolution* of the deflector, as it defines the number of "independent spots" (or "pixels") that can be addressed across the maximum deflection angle. Moreover, this parameter is invariant with respect to imaging optics. E.g. a telescope can be applied to increase the maximum deflection angle of the deflector, but will increase the beam divergence proportionally, such that the number of resolvable spots N remains unaffected.

Similarly, the maximum deflection angle velocity can be expressed in terms of the maximum *rate of resolvable spots* $\dot{N}$ (Bechtold et al., 2013b). This parameter can be understood as the rate, at which "independent spots" or "pixels" may be scanned over per unit of time. Again, the maximum deflection angle velocity may be changed using

optics (focussing lenses, telescopes, etc.), but the rate of resolvable spots remains constant and solely depends on the scanning technology. Table 1 lists typical values of deflection angle, speed and accuracy of different laser beam deflection technologies.

Besides the deflection angle, speed and accuracy, other properties determine the suitability of a deflector for a specific application, such as response time, damage threshold, size (aperture), range of wavelengths of the laser light that can be deflected, efficiency or transparency [%], power consumption (required voltages), and last but not least, the type and magnitude of beam distortions, such as astigmatism, introduced by the deflector.

Note that table 1 only lists typical values of laser beam scanners, which allow deflection of laser beams of a wavelength of $\lambda = 1\ \mu$m. Extending the table to other (ranges of) wavelengths would increase the data significantly, and was therefore omitted.

3. Electro-optical deflectors

An Electro-Optic Deflector (EOD), see Fig. 2, relies on the change of the refractive index n of a material as a result of an electric field E applied to an optically transparant material (Gottlieb et al., 1983; Maldonado, 1995; Scrymgeour et al., 2001). The latter is achieved by applying an electric voltage over the medium. The change of the refractive index is caused by electro-magnetic forces that perturb the position, orientation or shape of atom or molecule structure in the material. EODs refract a laser beam by introducing a phase delay across the cross section of the laser beam (Nakamura et al., 2006). Two types of electro-optic effects are distinguished. If the refractive index varies linearly with the electric field, such as in $LiNbO_3$, $LiTaO_3$ and $KTiOPO_4$ crystals, this electro-optic effect is referred to as the *Pockels effect* (Djukic et al., 2004; Scrymgeour et al., 2001; Chiu et al., 1996). If it varies quadratically with the field strength, so with E^2, it is referred to as the *Kerr effect* or *quadratic electro-optic* effect (QEO effect). All materials exhibit the Kerr effect, but it is usually much weaker than the Pockels effect. An exception is Potassium Tantalate Niobate ($KTa_{1-x}Nb_xO_3$, or short KTN), which shows a large electro-optic effect at a particular temperature, which depends on the ratio of Tantalate and Niobate (Wang et al., 1992; Chen et al., 1996). Therefore, this crystal is (to be) actively controlled to a temperature just above the Curie temperature (typically chosen via the Ta_{1-x}:Nb_x ratio to be approximately 35 °C), at which the Kerr constant is at its maximum (Nakamura et al., 2008; Wang et al., 1992). Then, at a field strength of 500V/mm the variation of the refractive index in a KTN crystal equals $1.52 \cdot 10^{-2}$, whereas at this field strength in a Lithium Niobate crystal (Pockels effect) the variation is only $9 \cdot 10^{-5}$ (Yagi, 2009). Therefore, EODs based on KTN crystals show a larger maximum deflection angle, as well as deflection velocity, than EODs based on the Pockels effect, see Table 1.

Fig. 2 shows the two typical configurations of Electro-Optic Deflectors. Fig. 2(a) shows an EOD based on refraction

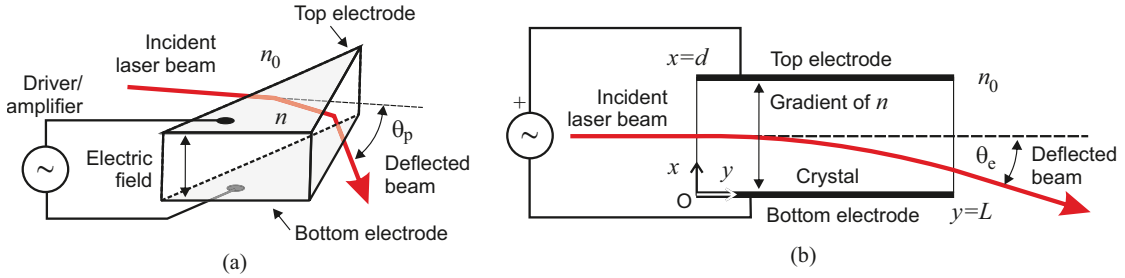

Fig. 2. Typical typical configurations of an Electro-Optic Deflectors. (a) EOD based on refraction at the interface(s) of an optical prism. Adapted from (Chen et al., 1996). (b) EOD based on refraction by an index gradient that exists perpendicular to the direction of the propagation of the laser beam. Adapted from (Yagi, 2009).

at the interface(s) of an optical prism, equipped with two electrodes and a driver/amplifier, inducing an electric field perpendicular to the electrodes. The angle of deflection θ_p is proportional to the width l of the base, and inverse proportional to the height w of the prism (Scrymgeour et al., 2001)

$$\theta_p = \frac{\Delta n}{n}\frac{l}{w}, \tag{2}$$

where n denotes the refractive index of the crystal and Δn the difference between the refractive index of the crystal and the surrounding material. By placing several prisms in sequence, the maximum deflection angle can be increased. Then the number of prisms and the dimensions of the individual prisms are optimized for large angle of deflection, high damage threshold and minimized reflection losses (Gottlieb et al., 1983; Maldonado, 1995). Note, that in this configuration, refraction (and therefore deflection) takes place at the interfaces of electro-optic and embedding material only. Therefore, maximum deflection angles are limited to a few degrees. Fig. 2(b) shows an EOD based on refraction by an index gradient that exists perpendicular to the direction of the propagation of the laser beam. Besides the electro-optic crystal, it consists of two electrodes and a driver/amplifier. In this configuration, the laser beam is cumulatively refracted as it propagates through the crystal. Deflectors based on Potassium Tantalate Niobate (KTN) crystals are of this type. As these crystals show a much larger maximum deflection angle, for a given field strength, than EODs based on other Kerr cells, or Pockels cells for that matter, only deflectors based on KTN crystals will be discussed below.

The fact that Potassium Tantalate Niobate (KTN) shows larger deflection than other materials, such as $BaTiO_3$, $SrTiO_3$, and $Sr_xBa_{1-x}Nb_2O_6$, at the same field strength, is attributed to a specific distribution of the electric field perpendicular to the beam propagation, not observed in other Kerr cells (Huang et al., 2014). This specific distribution is attributed to "trapped charges" inside the crystal, as a result of electrons injected into the crystal from the electrodes (Miyazu et al., 2011). This effect was referred to as the *space-charge effect* and is superimposed on the Kerr effect (Nakamura et al., 2008, 2006; Naganuma et al., 2009). Assuming the laser beam enters the crystal along the optical axis of the crystal, see Fig. 2(b), the angle of deflection, due to a voltage V over the KTN crystal, equals (Yagi, 2009; Nakamura et al., 2008)

$$\theta_e = -0.153 n^3 \epsilon_0^2 \epsilon_r^2 \frac{V^2}{d^3} L, \tag{3}$$

where ϵ_0 denotes the permittivity of vacuum, $\epsilon_r = 3 \cdot 10^4$ the relative permittivity and $n = 2.2$ the refractive index of KTN at $V = 0$, L denotes the propagation length of the laser beam in the crystal and finally d denotes the thickness of the crystal. The negative sign in equation (3) indicates that the laser beam is deflected towards the cathode. Hence, controlling the voltage allows to control the beam deflection angle. Substituting typical dimensions (d=1 mm and L=6mm) and voltage $V = \pm$ 400 volts shows that the typical maximum deflection angle equals $\theta_e = \mp 110$ mrad, which is indeed large compared to an EOD based on the Pockels effect, see Table 1. However, when compared to mirror based deflectors, the typical maximum deflection angle, as well as the aperture (size) of EODs, including those based on KTN crystals, are small, see Table 1. Hence, the number of resolvable spots is small, too. The latter is the main drawback of an EODs, when compared to mirror based scanners.

Compared to mirror based scanners, the angular accuracy of EODs is high, see Table 1. However, it should be noted that the availability of accuracy data is quite sparse. The deflection of the laser beam by an EOD based on the Kerr effect (only) is highly linear with the applied voltage, such that the accuracy is mainly determined by the accuracy of the high voltage driver, which is in the range of .1 % to 1%. Hence, depending on the maximum deflection accuracy, the angular accuracy of these EODs should be in a range of approximately 0.1 μrad to 10 μrad. For EODs based on the KTN crystal, accuracy data is even more scarce. Commercially available KTN based EODs tend to show an inaccuracy of approximately 10 mrad when varying the deflection angles between 0 and ±100 mrad (NTT, 2014).

A major advantage of KTN over other electro-optic crystals is that a relatively large deflection is achieved at relatively low voltage levels (typically 400 volts and less). In comparison, the sensitivity of other electro-optic media is in the order of 2 mrad/kV (Chiu et al., 1996). As the electro-optic crystal electrically appears as a capacitor, the amplifier is to be able to handle large currents when switching high voltages at high frequencies. Nevertheless, the maximum deflection angle velocity of EODs is (much) larger than of mirror based scanners, see Table 1. In addition, the random-access response time of EODs are smaller than the response time of mirror based scanners, as well as of Acousto-Optic Deflectors for that matter. The latter is due to the fact that a (changing) electric field in a crystal is established at the speed of light in the material, rather than at the acoustic velocity in the material, see equation (6).

By bonding a second pair of electrodes to the crystal, see Fig. 2(b), oriented orthogonally to the top and bottom electrodes, a *quadrupole deflector* is obtained (Gottlieb et al., 1983). With an additional driver/amplifier this allows to deflect the laser beam in two directions.

The damage threshold of KTN is larger than 1 J/cm^2 (Ellenberger et al., 1992), and it is transparent for light with a wavelength of 532 nm to 4000 nm (Bass, 2010). Unlike Acousto-Optic Deflectors, EODs do not suffer from diffraction

losses. Optical losses are due to reflection, absorption, and scattering and are less than 10% in total, see Table 1. Again unlike Acousto-Optic Deflectors, the deflection angle does not depend on the wavelength of the laser beam (compare equation (4) and (5)).

Bechtold et al. (2012) experimentally studied beam profile deformations in a KTN deflector, deflecting a 400 fs pulsed laser beam at a wavelength of 1064 nm. It was found that the KTN crystal introduces significant astigmatism to the beam of which the magnitude depends on the angle of deflection. In addition, it was found that the beam profile deformations in a KTN deflector depend on the laser fluence. The latter was attributed to a pertubation of the trapped charges in the KTN crystal, as a result of multiphoton absorption at fluence levels exceeding approximately 10 mJ/cm^2. This problem could be addressed by a crystal with a larger aperture to accommodate larger beam diameters.

4. Acousto-optical deflectors

An Acousto-Optic Deflector (AOD), see Fig. 3, is based on a periodically changing refractive index n in an optically transparant material (e.g. TeO_2 or $PbMoO_4$), induced by propagating sound waves in the material (Bullen et al., 1997; Chang, 1995; Xu and Stroud, 1992; Gottlieb et al., 1983). The changing refractive index is the result of rarefaction and compression of the material, inducing a changing density of the material. This periodically changing refractive index n acts like an optical grating, moving at the speed of sound in the crystal, that will diffract a laser beam traveling through the material (Tran, 1992).

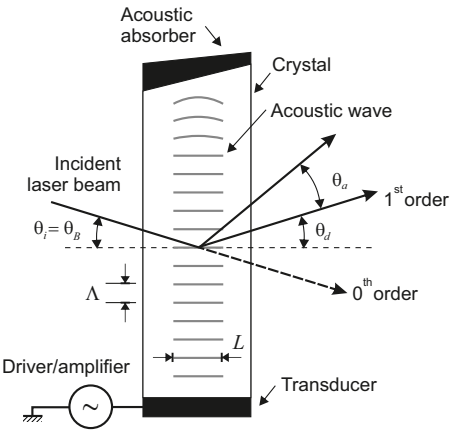

Fig. 3. Typical configuration of an Acousto-Optical Deflector (AOD). Adapted from Zeng et al. (2009).

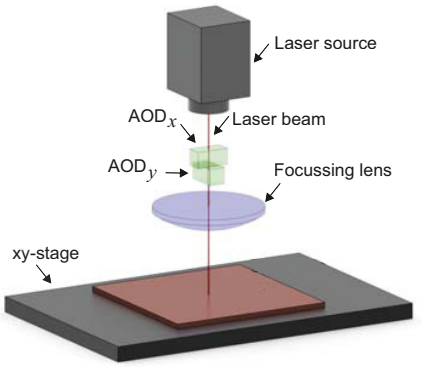

Fig. 4. A two-dimensional scanner can formed by arranging two OADs orthogonally in series.

Fig. 3 shows the typical configuration of an Acousto-Optic Deflector, consisting of the acousto-optic crystal to which a transducer (typically a piezo-electric element) is glued or deposited. Driven by an amplifier, the transducer launches acoustic waves, of frequency f_a (typically 80MHz to 1GHz depending on the material), into the crystal producing the grating. At the opposite end, the crystal is typically skew cut and fitted with an acoustic absorbing material to avoid reflection of the acoustic wave back into the crystal (Xu and Stroud, 1992). If the interaction length L is sufficiently long, and the laser beam is incident at the Bragg angle – i.e. $\theta_i = \theta_B \approx \lambda/(2\Lambda)$, with Λ the acoustic wavelength – with respect to the acoustic wavefront, only first order refraction of the light is observed, because higher order diffraction orders undergo destructive interference. The angle of deflection θ_d (outside the crystal, see Fig. 3) of the 1st order diffraction depends on the wavelength λ of the laser light in vacuum, the frequency f_a of the acoustic wave, n the refractive index of the unperturbed material and the velocity v_a (order of magnitude 10^2 m/s to 10^3 m/s) of the acoustic wave in the crystal,

$$\theta_d = \frac{\lambda f_a}{2 n v_a}. \tag{4}$$

Therefore, if the frequency of the sound wave is varied, while the incidence angle θ_i of the laser beam is fixed at $\theta_i = \theta_B$, the direction of the diffracted laser beam varies. Hence, the name Acousto-Optic Deflector. Changing the acoustic frequency from f_a to $f_a + \Delta f_a$, where Δf_a denotes the frequency bandwidth of the driver/amplifier, changes the deflection angle. Depending on the material, the frequency bandwidth typically ranges from 40MHz to 500MHz. Then, the maximum deflection angle θ_a of an AOD equals (see Fig. 3),

$$\theta_a = \frac{\lambda \Delta f_a}{2 n v_a}. \tag{5}$$

The frequency bandwidth Δf_a has a strong effect on the optical efficiency of deflection. That is, when the incident angle equals the deflection angle and thus the Bragg angle (i.e. $\theta_B = \theta_i = \theta_d$), the diffraction efficiency is at maximum. When the acoustic frequency f_a is increased, this condition is not fully met and the Bragg condition is increasingly violated. Usually, the frequency bandwidth Δf_a is chosen such that the diffraction efficiency does not fall below 50 % to 60 %. Several countermeasures, such as facetted and phase-shifted transducers (Chang (1995)), are used in commercially available AODs to increase the bandwidth Δf_a. When compared to mirror based deflectors, the typical maximum deflection angle θ_a, as well as the aperture (size) of AODs are small, see Table 1. Hence, the number of resolvable spots is small, too. The latter is the main drawback of an AOD, when compared to mirror based scanners.

Again compared to mirror based scanners, the angular accuracy of AODs is high, see Table 1. The frequency generators driving the transducers are typically digitally controlled – i.e. the acoustic frequency is resolved digitally in 8 bits up to 31 bits. A controlled frequency resolution of 1 Hz is quite common (AAOE, 2014). This corresponds to an angular accuracy of about 1.6 nrad for an AOD based on a TeO_2 crystal and $\lambda = 1064$ nm; and 0.15 nrad for a AOD based on Crystal Quartz and $\lambda = 355$ nm. Drift, common for Galvo-scanners, as well as temperature dependency in comparison to analogue controllers, are usually not problems encountered in AODs. This high angular accuracy of AODs implies that the mechanical mounting of the AODs is the main cause of angular inaccuracies.

Since it takes a finite time for the acoustic wave to fill the crystal, it takes time to "switch" from one specific acoustic frequency to the next, and therefore, from a specific angular direction of the deflected beam to the next. This settling time is referred to as the *response time* τ_a (or *transit time* or *random-access time*) of the AOD, and depends on the acoustic velocity v_a and on D, which denotes the beam diameter or the optical aperture of the AOD, whichever is smaller, as (Tran, 1992; Chang, 1995)

$$\tau_a = \frac{D}{v_a}. \tag{6}$$

The response time is also a measure of the deflection angle velocity of the AOD. That is, a small response time implies high deflection angle velocities. This implies that, the deflection angle velocity (rate of resolvable spots) of an AOD can be about a factor of 4 to 100 higher than of mirror based scanners, see Table 1. Unfortunately, materials exhibiting high diffraction efficiency, show a small optical damage threshold (Xu and Stroud, 1992; Gottlieb et al., 1983). To cope with the latter, requires AODs with large optical aperture to accommodate a large(r) beam diameter, but also requires more (electrical) power to drive the transducer. Typical cw damage thresholds range from 1MW/m^2 to 500MW/m^2, depending on the material. Unfortunately, increasing the size of the AOD, to increase the power handling capacity of the AOD, reduces the response time, as is obvious from equation (6). Further, materials exhibiting a low acoustic velocity v_a will provide large(r) angle of deflection, and therefore a large(r) number of resolvable spots. Consequently, the response time (6) of these materials is smal(ler). Hence, the design of an AOD is a compromise between between maximum deflection angle and speed. Nonetheless, when compared to mirror based deflectors, the response times of AODs are small, see Table 1. It should be noted that, during the transition from one frequency to the next, the angle of the deflected beam might be undefined. A work around for the latter is to synchronize the frequency switching with the pulse frequency of the laser beam, as demonstrated by Bechtold et al. (2013a).

As is clear from equations (4) and (5), the diffraction angle of an AOD depends of the wavelength of the laser beam. This implies a linear chromatic dispersion of laser beams with large spectral bandwidth, such as is the case with femtosecond laser pulses. This dispersion which may lead to deformed and enlarged structure geometry (Iyer et al., 2003; Ngoi et al., 2001). A second characteristic of an acousto-optic element to be taken into account is the energetic efficiency of the diffraction as function of the acoustic power. That is, the higher the acoustic power, the higher the optical intensity in the diffracted beam, and the lower the intensity in the zero order (i.e. non-diffracted) beam, see Fig. 3. The power in the latter beam is usually blocked/dumped. The associated *diffraction efficiency*

ranges typically from 55% to 75%. Hence, besides deflection, the AOD can also be used to effectively control (or modulate) the intensity and power of the deflected beam at high speed, which proves to be a useful attribute in a setup for laser material processing, see also section 5. Further optical transmission losses are typically 5% of the incident laser power.

An additional problem of AODs is that, as the speed of scanning is increased, the element introduces a cylindrical focusing effect (Xu and Stroud, 1992; Kirkby et al., 2010; Chang, 1995). That is, in the case of constant scanning sweeps, an acoustic wave with a constant frequency chirp is introduced into the acousto-optical crystal. Then, tracing the individual rays from the AOD would reveal that the focus location of the deflected beam, due to the frequency chirp, is similar to the focus location introduced by a laterally moving lens (VanderLugt and Bardos, 1992). This effect implies astigmatism of the laser beam. The effect can be compensated for by adding a cylindrical lens after the AOD, but this compensation can only be optimized for a single scan speed (Okabe et al., 2013). Therefore most approaches employ additional AODs inducing the inverse amount cylinder lensing (Bechtold et al., 2013a; Kirkby et al., 2010). However, Bechtold et al. (2013a) developed a method to prevent cylindrical focusing effect, without compensationg optics, by acoustical frequency jumps synchronized to the pulse-to-pulse pause.

An advantage of mirror-based scanners over AODs, as well as EODs for that matter, is the wide range of laser wavelengths that can be deflected. The latter is achieved by applying a coating on the mirror optimized for reflection at the selected wavelength. Like in the case of EODs, the crystal material of AODs determines the range of wavelengths that can be deflected. Popular AODs are based on TeO_2 crystals (350-5000 nm) and $PbMoO_4$ crystals (420-5500nm).

An AOD deflects the beam in one direction (plane). A two-dimensional scanner can formed by arranging two AODs orthogonally in series, as illustrated in Fig. 4.

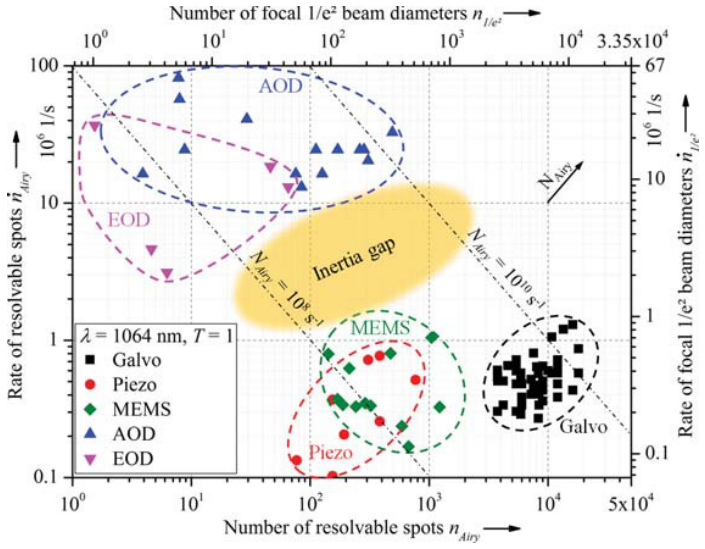

Fig. 5. Number and rate of resolvable spots and focal beam diameters $1/e^2$for $\lambda = 1064$ nm and $T = 1$. Reproduced from Bechtold et al. (2013b).

5. Combined optical and mechanical deflection

Fig. 5 shows the number of resolvable spots (related to the maximum angle of deflection) and rate of resolvable spots (related to the maximum deflection angle velocity) for random-access mirror based deflectors (Galvo, piezo, MEMS), as well as optical deflectors (EODs and AODs). Mirror based scanners are found in the lower right of this graph, which is characterized by a large number of resolvable spots, but by a low rate of resolvable spots. Vise versa, EODs and AODs are found in the upper left of this graph, which is characterized by relatively low number of resolvable spots, but by a high rate of resolvable spots.

Hence, this graph nicely illustrates that the performance of random-access mirror based scanners, in terms of maximum deflection angle velocity, is physically limited by the inertia associated with the rotating mirror and other moving parts of these scanners. This was referred to as the "inertia gap" by Bechtold et al. (2013b). This gap can be bridged by combining a mirror-based scanner with an optical deflector. That is, for applications requiring a scanner showing both a high number of resolvable spots and a high rate of resolvable spots, arranging a mechanical scanner and optical deflector in series allows to take advantage of the best of both worlds, see Fig. 6.

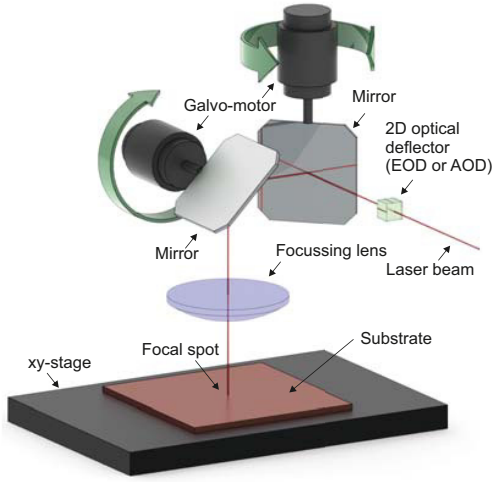

Fig. 6. Concept architecture of a laser beam scanner composed a mechanical scanner (here a Galvo-scanner) combined with an optical deflector.

In this combined architecture, the mechanical scanner deflects the laser beam at an angle of θ_{me}, see Fig. 7. This angle is measured by a position sensor(s), e.g. the encoders on the Galvo-motors, which gives θ_{m} and is subsequently compared to the desired or reference angle θ_{r}. Hence, the resulting signal $\theta_{\mathrm{e}} = \theta_{\mathrm{r}} - \theta_{\mathrm{m}}$ is the angular error introduced by the mechanical scanner. This signal, when multiplied by -1, acts as a reference signal for the optical deflector. In this configuration, the high speed optical deflector can swiftly, and in real-time, correct for angular errors introduced by the mechanical scanner. A prerequisite for this approach is that the maximum deflection range of the optical deflector is larger than the angular error θ_{e} of the mechanical scanner, and that the response time of the optical deflector is smaller than the dynamics of the angular error. This approach is known in Mechatronics as *large-stroke-small-stroke* (Fan et al., 2007). This architecture not only exhibits a higher angular accuracy, but can also be exploited to increase the maximum deflection range and/or velocity of the mechanical scanner, without deteriorating the overall angular accuracy of the combined scanner. In any case it allows to fully exploit the high-repetition-rate of modern ultra-short pulsed laser sources.

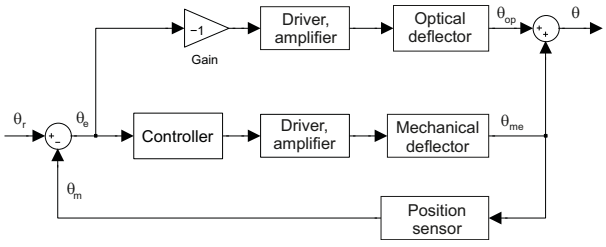

Fig. 7. Block diagram of combined mechanical and optical deflector.

Matsumoto et al. (2013) combined two AODs with a Galvo-scanner to increase the throughput of picosecond laser ablation for patterning of printed wiring boards. The two AODs were not only used to deflect the laser beam, but

also used to modulate the transmitted laser power at high speed, Unrath et al. (2010). It was shown that 1 mm square test patterns could be scanned at 4 m/s and an in-plane position accuracy of the focal spot of approximately 4 μm. Moreover, it was shown that the high pulse frequency of the laser source could be fully exploited by this architecture.

Full pulse-to-pulse separation (pulse overlap 0%) at 2 MHz repetition rate was achieved by Bruening et al. (2011) and Du et al. (2012) by dithering the laser spot using a single AOD. When using the AOD, the picosecond pulsed laser beam was deflected at 17 m/s horizontally, while the surface translated vertically at a constant speed of 1.3 m/s, resulting in a spatial pulse-to-pulse distance of 8.5 μm – the focal spot diameter was 9 μm. A pulse energy of 7 μJ was applied for microstructuring of several metals with no apparent burr or recast formation. This resulted in an ablation rate of 3 mm^3/min, which is an order of magnitude higher than achieved when employing a typical Galvo-scanner (same surface quality), compare e.g. Jaeggi et al. (2011). Hence, Bruening et al. (2011) and Du et al. (2012) showed the importance of high-speed deflection to increase the efficiency of laser microstructuring.

6. Conclusions

As Electro-Optical Deflectors (EODs) and Acousto-Optical Deflectors (AODs) do not include moving parts, high angular deflection velocities can be achieved, when compared to mechanical scanners. However, the maximum deflection angle, and more relevant, the number of resolvable spots of these optical deflectors is small, when compared to mechanical scanners. Nevertheless, the angular accuracy of EODs and AODs is high. Arranging an optical deflector (EOD or AOD) and a mechanical scanner in series allows to take advantage of the best of both worlds. In this approach, the angular deflection errors introduced by the mechanical scanner are compensated, in real-time, by optical deflector(s).

Acknowledgements

The authors gratefully acknowledge discussions with Ger Folkersma, Ewoud Biesheuvel and Hedzer Durksz.

References

AAOE, 2014. AA Opto-electronic, France. DDSPA variable frequency source - direct digital synthesizer. URL: `http://aaoptoelectronic.com/Documents/DDSPAXX-2011.pdf` (accessed June 2014).

Bass, M., 2010. Handbook of optics. 3 ed., McGraw-Hill, New York.

Bechtold, P., Bauer, D., Schmidt, M., 2012. Beam profile deformation of fs-laser pulses during electro-optic scanning with KTN crystals. Physics Procedia. Proceedings of the Laser Assisted Net shape Engineering 7 (LANE 2012) 39, 683–692.

Bechtold, P., Hohenstein, R., Schmidt, M., 2013a. Beam shaping and high-speed, cylinder-lens-free beam guiding using acousto-optical deflectors without additional compensation optics. Optics Express 21, 14627–146–35.

Bechtold, P., Hohenstein, R., Schmidt, M., 2013b. Evaluation of disparate laser beam deflection technologies by means of number and rate of resolvable spots. Optics Letters 38, 2934–2937.

Bruening, S., Hennig, G., Eifel, S., Gillner, A., 2011. Ultrafast scan techniques for 3D-μm structuring of metal surfaces with high repetitive ps-laser pulses. Physics Procedia. Proceedings of the Sixth International WLT Conference on Lasers in Manufacturing (LiM2011) 12, 105–115.

Bullen, A., Patel, S., Saggau, P., 1997. High-speed, random-access fluorescence microscopy: 1. high-resolution optical recording with voltage-sensitive dyes and ion indicators. Biophysical Journal 37, 477–491.

Chang, I., 1995. Handbook of optics. Volume II: Devices, Measurements, and Properties. chapter 12. pp. 12.1–12.54.

Chen, F., Geusic, J., Kurtz, S., Skinner, J., Wemple, S., 1996. Light modulation and beam deflection with Potassium Tantalate Niobate crystals. Journal of Applied Physics 37, 388–398.

Chiu, Y., Stancil, D.D., Schlesinger, T.E., Risk, W.P., 1996. Electro-optic beam scanner in $KTiOPO_4$. Applied Physics Letters 69, 3134 69, 3134–3136.

De Loor, R., 2013. Polygon scanner system for ultra short pulsed laser micro-machining applications. Proceedings of Lasers in Manufacturing (LiM) conference 2013, Physics Procedia 41, 544–551.

Djukic, D., Roth, R., Yardley, J.T., Jr., R.M.O., 2004. Low-voltage planar-waveguide electrooptic prism scanner in crystal-ion-sliced thin-film $LiNbO_3$. Optics express 12, 6159–6164.

Du, K., Brüning, S., Gillner, A., 2012. High power picosecond laser with 400w average power for large scale applications. Proc. SPIE 8244, Laser-based Micro- and Nanopackaging and Assembly VI , 82440P1–10.

Ellenberger, U., Weber, R., Balmer, J.E., Zysset, B., Eligehausen, D., Mizell, G.J., 1992. Pulsed optical damage threshold of potassium niobate. Applied Optics 31, 7563. doi:10.1364/AO.31.007563.

Fan, K.C., Lai, Z.F., Wu, P., Chen, Y.C., Chen, Y., Jäger, G., 2007. A displacement spindle in a micro/nano level. Measurement and science technology 18, 1710–1717.

Ferreira, L., Moehlecke, S., 1999. A silicon micromechanical galvanometric scanner. Sensors and Actuators A: Physical 73, 252–260. doi:10.1016/S0924-4247(98)00288-X.

Gottlieb, M., Ireland, C., Ley, J., 1983. Electro-optic and acousto-optic scanning and deflection. Marcel Dekker publishing, New York.

Huang, C., Sasaki, Y., Miyazu, J., Toyoda, S., Imai, T., Kobayashi, J., 2014. Trapped charge density analysis of KTN crystal by beam path measurement. Optics express 22, 7783–7789.

Iyer, V., Losavio, B.E., Saggau, P., 2003. Compensation of spatial and temporal dispersion for acousto-optic multiphoton laser-scanning microscopy. Journal of Biomedical Optics 8, 460–471. doi:10.1117/1.1580827.

Jaeggi, B., Neuenschwander, B., Schmid, M., Muralt, M., Zuercher, J., Hunziker, U., 2011. Influence of the pulse duration in the ps-regime on the ablation efficiency of metals. Physics Procedia 12, 164–171. doi:10.1016/j.phpro.2011.03.118.

Kirkby, P.A., Nadella, K.M.N.S., Silver, R.A., 2010. A compact acousto-optic lens for 2D and 3D femtosecond based 2-photon microscopy. Optics Express 18, 13721–13745.

Maldonado, T.A., 1995. Handbook of optics. Volume II: Devices, Measurements, and Properties. chapter 13. pp. 13.1–13.35.

Matsumoto, H., Unrath, M., Zhang, H., Hainsey, B., 2013. Laser direct ablation for patterning printed wiring boards using ultra-fast lasers and high speed beam delivery architectures. Journal of Laser Micro/Nanoengineering 8, 315–320.

Miyazu, J., Imai, T., Toyoda, S., Sasaura, M., Yagi, S., Kato, K., Sasaki, Y., Fujiura, K., 2011. New beam scanning model for high-speed operation using $kta_{1-x}nb_xo_3$ crystals. Applied Physics Express 4, 111501.

Naganuma, K., Miyazu, J., Yagi, S., 2009. High resolution ktn optical beam scanner. NTT technical review 17, 1–6.

Nakamura, K., Miyazu, J., Sasaki, Y., Imai, T., Sasaura, M., Fujiura, K., 2008. Space-charge-controlled electro-optic effect: optical beam deflection by electro-optic effect and space-charge-controlled electrical conduction. Journal of Applied Physics 104, 013105 (2008) 104, 013105.

Nakamura, K., Miyazu, J., Sasaura, M., Fujiura, K., 2006. Wide-angle, low-voltage electro-optic beam deflection based on space-charge-controlled mode of electrical conduction in $KTa_{1-x}Nb_xO_3$. Applied Physics Letters 89, 131115.

Ngoi, B.A., Venkatakrishnan, K., Lim, L., Tan, B., 2001. Angular dispersion compensation for acousto-optic devices used for ultrashort-pulsed laser micromachining. Optics Express 9, 200–206. doi:10.1364/OE.9.000200.

NTT, 2014. NTT Advanced Technology corp., Japan. KTN Deflector. URL: `http://www.ntt-at.com/product/ktn_scanner/` (accessed June 2014).

Okabe, Y., Sasaki, Y., Ueno, M., Sakamoto, T., Toyoda, S., Kobayashi, J., Ohmi, M., 2013. High-speed optical coherence tomography system using a 200-kHz swept light source with a KTN deflector. Optics and Photonics Journal 3, 190–193.

PI, 2014. Physik Instrumente (PI) GmbH & Co.KG, Germany. Piezo tip/tilt mirrors & scanners: Fundamentals. URL: `http://www.physikinstrumente.com/en/products/prdetail.php?sortnr=300300` (accessed June 2014).

Piyawattanametha, W., Patterson, P., Hah, D., Toshiyoshi, H., Wu, M., 2005. Surface- and bulk- micromachined two-dimensional scanner driven by angular vertical comb actuators. Journal of Microelectromechanical Systems 14, 1329–1338. doi:10.1109/JMEMS.2005.859073.

Schille, J., Ebert, R., Regenfuss, P., Suess, T., Exner, H., 2008. Micro structuring with highly repetitive ultra short laser pulses, in: Proceedings of the 9th International Symposium on Laser Precision Microfabrication (LPM2008). Québec, Canada, pp. 1–6.

Scrymgeour, D.A., Barad, Y., Gopalan, V., Gahagan, K.T., Jia, Q., Mitchell, T.E., Robinson, J.M., 2001. Large-angle electro-optic laser scanner on $LiTaO_3$ fabricated by in situ monitoring of ferroelectric-domain micropatterning. Applied optics 40, 6236–6241.

Tran, C.D., 1992. Acousto-optic devices, optical elements for spectroscopy. Analytical chemistry 64, 971–981.

Unrath, M., Jordens, W.J., Ismail, J., Matsumoto, H., Lineburg, B.J., 2010. Acousto-optic deflector applications in laser processing of dielectric or other materials (US patent N^o 2010301023).

VanderLugt, A., Bardos, A.M., 1992. Design relationships for acousto-optic scanning systems. Applied Optics 31, 4058–4068.

Wang, J., Guan, Q., Wei, J., Wang, M., Liu, Y., 1992. Growth and characterisation of cubic $KTa_{1-x}Nb_xO_3$. Journal of crystal growth 116, 27–36.

Xu, J., Stroud, R., 1992. Acousto-optic devices. Principles, Design, and applications. Wiley.

Yagi, S., 2009. KTN crystals open up new possibilities and applications. NTT technical review 7, 1–5.

Yalcinkaya, A., Urey, H., Brown, D., Montague, T., Sprague, R., 2006. Two-axis electromagnetic microscanner for high resolution displays. Journal of Microelectromechanical Systems 15, 786–794.

Zeng, S., Luo, Q., Li, D., Lü, X., 2009. Femtosecond pulse laser scanning using acousto-optic deflector. Science in China Series G: Physics, Mechanics and Astronomy 52, 685–692.